



Contents lists available at ScienceDirect

## Advanced Powder Technology

journal homepage: [www.elsevier.com/locate/apt](http://www.elsevier.com/locate/apt)

Original Research Paper

# Numerical simulation and sensitivity analysis of effective parameters on heat transfer and homogeneity of Al<sub>2</sub>O<sub>3</sub> nanofluid in a channel using DPM and RSM

Kamel Milani Shirvan<sup>a</sup>, Mojtaba Mamourian<sup>a,\*</sup>, Soroush Mirzakhani<sup>b</sup>, Hakan F. Öztöp<sup>c,d</sup>, Nidal Abu-Hamdeh<sup>d</sup>

<sup>a</sup> Department of Mechanical Engineering, Ferdowsi University of Mashhad, Mashhad, Iran

<sup>b</sup> Department of Mechanical and Aerospace Engineering, Science and Research Branch, Islamic Azad University, Tehran, Iran

<sup>c</sup> Department of Mechanical Engineering, Technology Faculty, Firat University, Elazig, Turkey

<sup>d</sup> Department of Mechanical Engineering, King Abdulaziz University, Jeddah, Saudi Arabia

## ARTICLE INFO

## Article history:

Received 15 March 2016

Received in revised form 21 May 2016

Accepted 28 June 2016

Available online xxx

## Keywords:

Response surface methodology

Sensitivity analysis

Discrete Phase Model

Heat transfer

Homogeneity of nanofluid

## ABSTRACT

In this paper, a 2-D numerical study and a sensitivity analysis of convective heat transfer in a channel are investigated using the Discrete Phase Model along with determination of the nanoparticles concentration distribution. Numerical simulations are carried out to investigate the effects of the three parameters, the Reynolds number ( $250 \leq Re \leq 650$ ), nanoparticles volume fraction ( $0.01 \leq \phi \leq 0.05$ ) and nanoparticles diameter ( $40 \text{ nm} \leq dp \leq 100 \text{ nm}$ ) on the heat transfer performance and nanoparticles distribution. In addition, the effective parameters analysis is performed utilizing the Response Surface Methodology. The results indicated that increasing the  $Re$  number and  $\phi$  and decreasing of  $dp$ , enhances the mean total Nusselt number. Also, an enhancement in  $dp$  and  $\phi$  and reduction of  $Re$  number increases the homogeneity of the nano-fluid. In addition, it is found that the sensitivity of the mean total Nusselt number to  $Re$  number,  $\phi$  and  $dp$  parameters is more than the sensitivity of the nanoparticles concentration ratio to these parameters.

© 2016 The Society of Powder Technology Japan. Published by Elsevier B.V. and The Society of Powder Technology Japan. All rights reserved.

## 1. Introduction

Several applications of thermal engineering in solar heat exchangers, cooling of electronic equipment, compact heat exchangers, thermal-energy conversion devices and solar collectors are some examples of various important practical applications and usage of forced convection heat transfer in channels. Therefore, during the process of the heat transfer in channels investigation, the predicting of the heat transfer is one of the basic essentials. Enhancing of the heat transfer in above mentioned engineering applications has been a subject of interest in several research studies in last years. Also, due to the low thermal conductivity of the common fluids which are used in commercial applications of channels (including water, ethylene glycol and oil), to improve the heat transfer rate, adding of nanoparticles such as Cu, Al<sub>2</sub>O<sub>3</sub> and TiO<sub>2</sub> to the fluid which creates a mixture called nanofluid and enhances the heat transfer coefficient, has been investigated in several papers [1–5].

Nanofluids have various applications in fluids and heat transfer studies. As mentioned above, some researchers have considered the effects of the adding nanoparticles to enhance the heat transfer rate. These researches were mostly done by considering a single phase and some of them by two phases; such as the study which was done by Bianco et al. [2] on the turbulent convection heat transfer of Al<sub>2</sub>O<sub>3</sub>-water nanofluid in a circular tube subjected to constant wall temperature. In their study, the numerical investigation was done using the mixture model that is an appropriate method to simulate nanofluids behavior. The results showed that increasing of the nanofluid concentration increases the Nusselt number. Another numerical study on flow characteristics, heat transfer and entropy generation of nano-fluid flow inside an annular pipe partially or completely filled with porous media using two-phase mixture model has been carried out by Siavashi et al. [3]. They found that the Reynolds number, nanoparticles concentration and configurations parameters, have significant effects on the entropy generation and the performance. Bianco et al. [4] have investigated a numerical study on entropy generation of turbulent convection flow of a nano-fluid in a circular tube under a constant heat flux. The results revealed that increasing the  $Re$  number

\* Corresponding author at: P.O.B. 91775-1111, Mashhad, Iran.

E-mail address: [mamourian@um.ac.ir](mailto:mamourian@um.ac.ir) (M. Mamourian).

**Nomenclature**

$C_p$	specific heat ( $\text{J kg}^{-1} \text{K}^{-1}$ )	$X, Y$	dimensionless Cartesian coordinates
$dp$	nano-particle diameter (nm)	<i>Greek symbols</i>	
$d_{ij}$	the tensor of deformation	$\alpha$	thermal diffusivity, $k/(\rho c_p)$ ( $\text{m}^2 \text{s}^{-1}$ )
DPM	Discrete Phase Model	$\beta$	thermal expansion coefficient ( $\text{K}^{-1}$ )
$F_{ij}$	view factor between surfaces $i$ and $j$	$\lambda$	fluid mean free path (m)
$F_T$	the thermophoretic force	$\theta$	dimensionless temperature
$g$	gravitational acceleration ( $\text{m s}^{-2}$ )	$\mu$	dynamic viscosity (Pa s)
$h$	the convection heat transfer coefficient	$\nu$	kinematics viscosity ( $\text{m}^2 \text{s}^{-1}$ )
$H$	the height and width of the cavity (m)	$\rho$	density ( $\text{kg m}^{-3}$ )
$k$	thermal conductivity ( $\text{W m}^{-1} \text{K}^{-1}$ )	$\delta V$	cell volume ( $\text{m}^3$ )
$Kn$	Knudsen number	<i>Subscripts</i>	
$L$	heat exchanger length (m)	$B$	Brownian
$S_{n,ij}$	the spectral intensity	$D$	drag
$Nu$	local Nusselt number	$f$	base-fluid
$P$	pressure ( $\text{N m}^{-2}$ )	$O$	inlet
$P$	dimensionless pressure	$L$	lift
$Pr$	Prandtl number	$m$	momentum
$q_0''$	heat flux ( $\text{W m}^{-2}$ )	$p$	particle-pressure
$Re$	Reynolds number	$t$	total
$T$	temperature (K)	$T$	thermophoretic
$u, v$	velocity components along $x$ -axis and $y$ -axis, respectively ( $\text{m s}^{-1}$ )	$v$	viscous
$U, V$	dimensionless of velocity component	$w$	wall
$x, y$	$x$ - and $y$ -axis coordinates, respectively		

decreases the optimal particles concentration to minimize entropy generation. Huang et al. [5] have carried out an experimental investigation on heat transfer and pressure drop characteristics of  $\text{Al}_2\text{O}_3$ /water and MWCNT/water nano-fluids flowing in a chevron-type plate heat exchanger. They found that utilizing of nano-fluids at constant Reynolds number, increases the heat transfer. An investigation to evaluate the performance of two types of nanofluids on the heat transfer in the context of the compact channels has been done by Haridas et al. [6]. In addition, experiments have been carried out in forced convection regime for a range of Reynolds numbers. Rahimi-Gorji et al. [7] have performed an analytical study on the heat transfer for the micro-channel heat sink (MCHS) using the porous media approach and the Galerkin method. The micro-channel heat sink was cooled using different nanofluids (Cu,  $\text{Al}_2\text{O}_3$ , Ag,  $\text{TiO}_2$  as nanoparticles and water and ethylene glycol as base fluids). The results revealed that, increasing the nanoparticles volume fraction enhances the Brownian movement of the particles, and consequently, reduces the difference between coolant and wall temperature. An experimental investigation on the characteristic of flow and heat transfer of  $\text{Al}_2\text{O}_3$ -water nanofluids flowing through a micro heat sink has been carried out by Zhai et al. [8]. In this paper, the micro heat sink is assumed to have a complex structure and is under constant heat flux. Another experimental and numerical study on laminar convective heat transfer of water-based  $\text{TiO}_2$ -nanofluid flowing through a heat exchanger has been carried out by Ebrahimnia-Bajestan et al. [9]. The results showed a maximum increase of 21% in average heat transfer coefficient utilizing the  $\text{TiO}_2$ /water nanofluids. Qi et al. [10] have investigated a numerical study on the flow and heat transfer of liquid metal based nanofluid with different nanoparticle radiuses using two-phase lattice Boltzmann method. The results indicated a considerable increase in the heat transfer of the nanofluid with small nanoparticle radius in comparison with the one with big nanoparticle radius. The reason is that at the same nanoparticle volume fraction, entire heat transfer surface area of all nanoparticles with small radius is higher than that of all nanoparticles with big radius; therefore, the heat transfer between particles increases with increasing of heat transfer surface

area and enhances the Nusselt number. A theoretically study on the nanoparticle migration effects on mixed convection of alumina/water nanofluid in a vertical micro-channel with considering of heat source/sink and asymmetric heating wall has been investigated by Malvandi et al. [11]. They found that the concentration-dependent buoyancy effects have considerable effects on flow and heat transfer characteristics. Also, imposed thermal asymmetry deformed the symmetry of velocity, temperature and nanoparticle volume fraction profiles and changed the direction of nanoparticle migration. Mirfendereski et al. [12] have carried out a numerical and experimental study on the laminar, steady state flow in helical tubes with considering of constant wall heat flux boundary condition. They found that utilizing of Ag nanofluid enhances the heat transfer of helical heat exchangers about 3.5–3.8%. A comparison between several models of viscosity of turbulent forced convection of  $\text{Al}_2\text{O}_3$  nanofluid over a heated cavity in a horizontal duct has been done numerically by Abdellahoum et al. [13]. The results revealed that increasing in volume fraction of nanoparticles enhances mean Nusselt number for whole range of Reynolds number. Malvandi and Ganji [14] have investigated a theoretical study on force convective heat transfer of alumina/water nanofluid inside a cooled parallel-plate channel with considering of the creeping flow regime and the presence of heat generation. They found that nanoparticles move from the adiabatic wall (nanoparticles depletion) toward the cold wall (nanoparticles accumulation) and construct a non-uniform nanoparticle distribution.

Another important model to simulate the nanofluids flow and heat transfer is the discrete phase model (DPM). In fact, in this model, the procedure is to track the particles individually utilizing the Lagrangian trajectory analysis method and to simulate the base-fluid the Eulerian frame is using. Among the researches about this field, we can mention the following studies: Selimefendigil et al. [15] have investigated a numerical study on mixed convection in a square cavity filled with  $\text{SiO}_2$  nanofluid and volumetric heat generation with considering of the effect of an inner rotating cylinder and a flexible side wall. In this paper, to depict the fluid motion with the flexible wall of the cavity in the fluid-structure

interaction model, the Arbitrary Lagrangian–Eulerian method is utilized. The results showed that by increasing the external and internal Rayleigh numbers, and reduction of elastic modulus of the flexible wall, the local and averaged heat transfer enhances. Also, the averaged heat transfer increases with cylinder rotation in both directions for all nanoparticle types. In another paper, a numerical simulation of nanofluid motion has been done by Jin [16] utilizing the Eulerian–Lagrangian method for both laminar and turbulent flow fields. The results indicated that for fully developed laminar flow regime, the nanoparticles follow the streamlines but for developing laminar regime, they have tendency to migrate toward the center. Afshar et al. [17] used this method to study the dispersion of nanoparticles in slip flow regime for a fluid flow in a micro-channel. The results revealed that by decreasing the particle diameter the heat transfer increases which is probably because of enhancement in surface area to volume ratio of solid phase. Another study on  $\text{Al}_2\text{O}_3$ –water nanofluid flow in a pipe was performed by Aminfar and Motallebzadeh [18] utilizing the discrete particle approach. They found that for low temperature gradients, the thermophoretic force has negligible effect on radial particle velocity. In another study, Bianco et al. [19] considered the forced convection of  $\text{Al}_2\text{O}_3$ –water nanofluid in circular tubes. The discrete particle model was also used in this paper. They found that adding nanoparticles reduces the wall and bulk temperatures. In addition to the mentioned studies, other researches have been done both numerically and experimentally using the DPM including Refs. [20,21]. Also, Rahimi-Gorji et al. [22] studied a numerical investigation on the airflow behavior and particle transport and deposition in various breathing conditions. To evaluate the transport and deposition of inhaled micro-particles, the Lagrangian method is utilized. The results revealed that the maximum value of the particle deposition fraction occurs for the case with  $dp = 5 \mu\text{m}$  and  $10 \mu\text{m}$  and the flow rate of  $30 \text{ L/min}$ , and also for the case with  $dp = 1 \mu\text{m}$  and the flow rate of  $15 \text{ L/min}$ .

Most of the earlier published researches, which some of them are mentioned in literature review section, have been investigated on the effects of the effective parameters, separately or as a combination of them such as: the Reynolds number [3–5], nanoparticles volume fraction [2,3,7] and the nanoparticles diameter [10,17]. According to the best knowledge of the authors, a numerical investigation on sensitivity analysis of all these three effective parameters on heat transfer and homogeneity in a channel filled with  $\text{Al}_2\text{O}_3$  nanofluid has not yet been considered.

The present investigation aims to obtain the optimal conditions to enhance the heat transfer rate (with investigating of mean  $Nu$  number) and homogeneity of nanofluid in a channel, which may provide a useful guideline for researchers of energy related fields. Therefore, the Reynolds number ( $Re$ ), nanoparticles volume fraction ( $\phi$ ) and the nanoparticles diameter ( $dp$ ) are obtained as the

effective parameters on the heat transfer performance and nanoparticles concentration distribution, and sensitivity analysis in a channel filled with  $\text{Al}_2\text{O}_3$  nanofluid is investigated in this paper using the discrete phase model.

In general, the novel issues in this article arise from the investigation of the optimal conditions and also sensitivity analysis of the forced convection heat transfer rate and homogeneity of nanofluid in a channel filled with  $\text{Al}_2\text{O}_3$  nanofluid using the DPM and Response Surface Methodology (RSM) models.

## 2. Problem statement

Fig. 1 indicates the geometry of the studied channel which has two horizontal walls. The geometry is composed of two parallel plates with height  $H$  and length  $L$  ( $\frac{H}{L} = 10$ ). The top and bottom walls of the channel are assumed to be adiabatic except for a part of the bottom wall that is under a uniform heat flux  $q''$ . The base fluid flow enters the channel with uniform velocity and temperature  $U_0$  and  $T_0$ , respectively, and the particles inlet temperature is  $300 \text{ K}$ .

## 3. Governing equations and mathematical model

In this paper, the convection heat transfer of a nanofluid flow within a channel under a partially uniform heat flux has been investigated. The nanofluid is assumed to be composed of water as base fluid and  $\text{Al}_2\text{O}_3$  with diameter of  $100 \text{ nm}$  as nanoparticle. Also, the fluid is considered as a continuous phase with dispersed particles inside. To study the particle distribution and thermal features of the suspensions containing the  $\text{Al}_2\text{O}_3$  nanoparticles, the two-phase Lagrangian–Eulerian model (Discrete Phase Model) is utilized. In other words, in this method, the particles are individually tracked using the Lagrangian frame, while the fluid is evaluated by the Eulerian frame. The interactions between the particles and fluid are considered as the source terms in momentum and energy equations. Also for the present set of computational simulations, some assumptions are made as follows:

1. The fluid is incompressible.
2. The Saffman's lift force and gravitational, Brownian, Thermophoretic and drag forces are considered included and the external forces are excluded. Since the nano-particles volume fraction is relatively low ( $\leq 5\%$ ), the particle–particle direct impacts are ignored. However, the particle–wall impacts are included in the analysis [23].
3. The two-way coupling between fluid and particle phase is carried out. The fluid phase (water) and the solid phase ( $\text{Al}_2\text{O}_3$  particles) interactions are completely considered in this two-way coupled model [23].

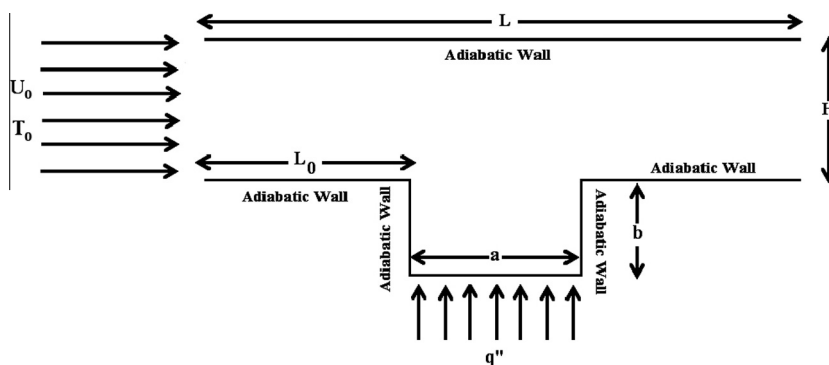


Fig. 1. The schematic of the channel.

4. Physical properties of Al<sub>2</sub>O<sub>3</sub> nanoparticles are considered as density  $\rho = 3970$  (kg m<sup>-3</sup>), thermal conductivity  $k = 40$  (W m<sup>-1</sup> K<sup>-1</sup>) and specific heat  $C_p = 765$  (J kg<sup>-1</sup> k<sup>-1</sup>) [23].
5. To investigate the enhancement of the heat transfer, the mean *Nu* number is calculated on the hot wall.
6. For the volume fraction of 1%, the average distance between nanoparticles is about 1000 nm, and this distance is 580 nm for 5% volume fractions. So, the probability of nanoparticles collisions for small volume fractions is small and negligible, and as a result, is neglected in this paper [23].
7. According to inconsiderable shares of inter-particle forces including the Van der Waals and electrostatic forces in nanofluids, the effect of them are ignored in this analysis [24].

Hence, with considering of above mentioned assumptions, the steady-state governing equations for the continuous phase are given as follows [23]:

Continuity equation:

$$\nabla \cdot (\rho_f v_f) = 0 \tag{1}$$

Momentum equation:

$$\nabla \cdot (\rho_f v_f v_f) = -\nabla P + \mu_f \nabla^2 \cdot v_f + S_{p,m} \tag{2}$$

Energy equation:

$$\nabla \cdot (\rho_f C_{p,f} v_f T_f) = \nabla \cdot (K_f \nabla T_f) + S_{p,e} \tag{3}$$

where subscript “*f*” refers to continuous phase and  $\rho$ ,  $k$  and  $C_p$  are density, thermal conductivity and specific heat, respectively; also,  $\mu$ ,  $V$ ,  $T$ , and  $P$  present the dynamic viscosity, velocity, temperature and pressure, respectively. In addition,  $S_{p,m}$  in Eq. (2) and  $S_{p,e}$  in Eq. (3) are the source terms which define the momentum and energy transfers between the fluid and the particles, respectively and can be calculated from the momentum and energy variations of the particles as they pass through the fluid phase of control volume.  $S_{p,m}$  and  $S_{p,e}$  are presented as follows [25]:

$$S_{p,m} = \sum n_p \frac{m_p}{\delta V} F \tag{4}$$

$$S_{p,e} = \sum n_p \frac{m_p}{\delta V} C_p \frac{dT_p}{dt} \tag{5}$$

where subscript “*p*” refers to particle and  $m_p$  and  $F$  are the particle mass and the total force per unit mass of the particle acting on it, respectively; also,  $\delta V$ ,  $n_p$  and  $t$  are the cell volume, number of solid particles within a cell volume and the time, respectively. Energy equation for the particle is given as follows:

$$m_p C_{p,p} \frac{dT_p}{dt} = Nu_p \pi d_p k_f (T_f - T_p) \tag{6}$$

Here  $d_p$  is the particle diameter and  $Nu_p$  is calculated by the Ranz and Marshall’s equation [26] as follows:

$$Nu_p = 2.0 + 0.6 Re_p^{0.5} Pr^{0.3} \tag{7}$$

where  $Re_p$  is the particle Reynolds number and  $Pr$  represents the Prandtl number. The total force  $F$  in Eq. (4) is consisted of the body and various hydrodynamic forces, which comprises the effects of the Saffman’s lift force, Brownian, thermophoretic and drag forces.

$$F = F_D + F_L + F_T + F_B \tag{8}$$

Here  $F_D$  can be calculated using different formulas, for instance, a form of Stokes drag law for sub-micron particles can be utilized [27] which gives the drag force  $F_D$  as follows:

$$F_D = \frac{18\mu_f}{d_p^2 \rho_p C_c} (v_f - v_p) \tag{9}$$

where  $C_c$  is Cunningham correction factor to Stokes drag law, which can be calculated from the below correlation [23]:

$$C_c = 1 + \frac{2\lambda}{d_p} (1.257 + 0.4e^{-(1.1d_p/2\lambda)}) \tag{10}$$

where  $\lambda$  is the molecular mean free path ( $\lambda = 0.17$  nm).

The Saffman lift force ( $F_L$ ) which is suggested for small particle Reynolds numbers, is due to a pressure distribution developed on the particle because of the rotation induced by a velocity distribution [28].

$$F_L = \frac{2K_s v^{1/2} \rho_f d_{ij}}{\rho_p d_p (d_{ij} d_{ij})^{1/4}} (v_f - v_p) \tag{11}$$

Here  $d_{ij}$  is the tensor of the deformation and  $K_s = 2.594$ . Due to the temperature gradient in the continuous phase, the thermophoretic force ( $F_T$ ) appears. The higher molecular velocities on one side of a particle, caused by the greater temperature, increase the momentum exchange and produce a force toward lower temperatures. The thermophoretic force [29] is calculated using the following:

$$F_T = -6\pi\mu_f^2 d_p C_s \frac{1}{\rho_f (1 + 3C_m Kn)} \frac{k_f/k_p + C_t Kn}{1 + 2k_f/k_p + 2C_t Kn} \frac{\nabla T}{m_p T} \tag{12}$$

where  $C_s = 1.17$ ,  $C_m = 1.14$ , and  $C_t = 2.18$ .

Also, it should be noted that, the effects of Brownian motion for particles smaller than micron can be comprised in the additional force term. The Brownian force is defined as follows:

$$F_B = \zeta \left( \frac{\pi S_0}{\Delta t} \right) \tag{13}$$

Here  $\zeta$  is the unit-variance-independent Gaussian random number, with zero mean value. Different components of the Brownian force  $F_B$  are modeled as a Gaussian white noise process, while the spectral intensity of  $S_{n,ij}$  is presented by Li and Ahmadi as follows [30]:

$$S_{n,ij} = S_0 \delta_{ij} \tag{14}$$

where  $\delta_{ij}$  is the Kronecker delta function, and  $S_0$  is:

$$S_0 = \frac{21\nu k_B T}{\pi^2 \rho_f d_p^5 \left(\frac{\rho_p}{\rho_f}\right)^2 C_c} \tag{15}$$

where  $\nu$  and  $k_B$  are the kinematic viscosity and the Boltzmann constant ( $1.3807 \times 10^{-23}$  J/K), respectively.

Finally, the local Nusselt number (*Nu*) of the hot wall is considered as:

$$Nu = \frac{hH}{k} \tag{16}$$

Here  $h$  is the convection heat transfer coefficient which can be obtained from:

$$h = \frac{q''_w}{T_w - T_i} \tag{17}$$

In which the subscript “*w*” indicates the surface temperature. Substituting Eq. (17) into Eq. (16) gives:

$$Nu_x = \frac{1}{\theta_w} \tag{18}$$

where  $\theta_w$  is a non-dimensional parameter and is calculated as follows:

$$\theta_w = \frac{(T_w - T_i)k}{q''H} \tag{19}$$

The mean total Nusselt number of the hot wall is defined by considering of the following equation:

$$Nu_{mt} = \frac{1}{A} \int NudA \tag{20}$$

### 3.1. Boundary conditions

As indicated in Fig. 1, the top and bottom walls of the channel are assumed to be adiabatic except for a part of bottom wall, which is assumed to be under uniform heat flux. At the inlet of the channel, the uniform distribution of the temperature is considered for both the fluid and the nanoparticles; also, a zero gradient (out flow) is applied at the outlet; and a no-slip and reflecting conditions are applied to the wall for the liquid phase and to the nanoparticles, respectively. Therefore, the boundary conditions are defined as follows:

Inlet:

$$u = U_0, \quad T = T_0 \quad (21)$$

Top wall:

$$u = v = 0, \quad \frac{\partial T}{\partial y} = 0 \quad (22)$$

Outlet:

$$\frac{\partial u}{\partial x} = \frac{\partial v}{\partial x} = 0, \quad \frac{\partial T}{\partial x} = 0 \quad (23)$$

Bottom wall:

$$u = v = 0, \quad \frac{\partial T}{\partial y} = 0 \quad (24)$$

$$u = v = 0, \quad q'' = 500 \text{ W/m}^2 \quad L_0 \leq x \leq L_0 + a$$

In addition, the reflect boundary condition is utilized for the top and bottom walls and the escape boundary condition is assumed for the inlet and outlet of the domain. Also, the particles inlet temperature is considered to be 300 K.

## 4. Numerical solution and validation

To obtain the governing equations (the mass, momentum and the energy conservation) numerically for the fluid and nanoparticle phases considering the boundary conditions and interphase correlations, the finite volume method (FVM) is used in this paper. In addition, using the second order upwind scheme, the convection term in the governing equations is discretized and the velocity and pressure fields are coupled utilizing the SIMPLE (Semi-Implicit Method for Pressure-Linked Equations) algorithm. The convergence criterion of the summation residual has been assumed to be less than  $10^{-7}$ . Moreover, discretization of the computational domain has been performed utilizing the structured non-uniform grids. The grids are finer close near to the heated wall where more accurate solutions are needed. The grid is stretched with  $\delta r = 0.02$  near walls to refine. Also, a grid independency investigation is done by considering the value of the calculated mean Nusselt number to check for the independency of the results from the number of the used grid points. Therefore, various numbers of grid points in  $x$  and  $y$  directions are used. The results of the flow with Reynolds number of 250 and  $\phi = 0.01$  are presented in Fig. 2.

According to the percentage of the difference between the values of the Nusselt number in studied grids, the number of the grid points in  $x$  and  $y$  directions are considered to be 35 and 100, respectively. The gridded solution field of channel is indicated in Fig. 3. As mentioned above, the grids are finer close to the wall which is under constant heat flux.

In order to validate the numerical model, the results of this study have been compared with Heyhat et al.'s [31] experimental data. The comparison was done for nanofluids flow under a laminar regime through a horizontal circular channel with a constant wall temperature.  $\text{Al}_2\text{O}_3$  nanoparticles with 40 nm diameter and

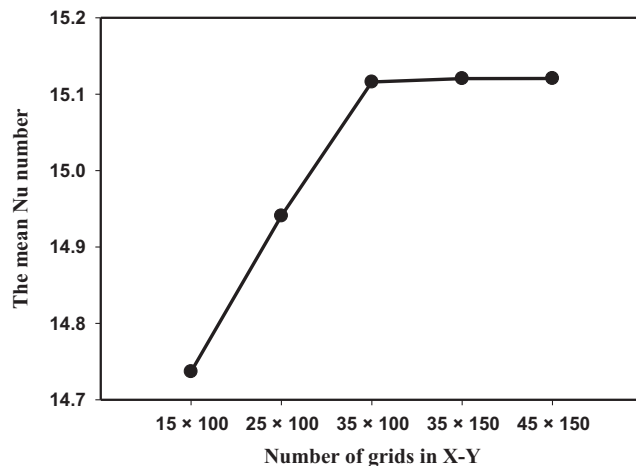


Fig. 2. The results of the mean Nusselt number on the hot wall to evaluate the grid independency.

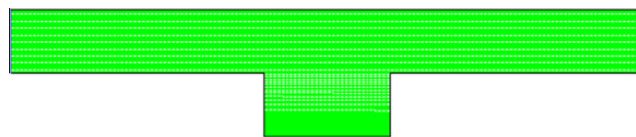


Fig. 3. The grids of the solution field.

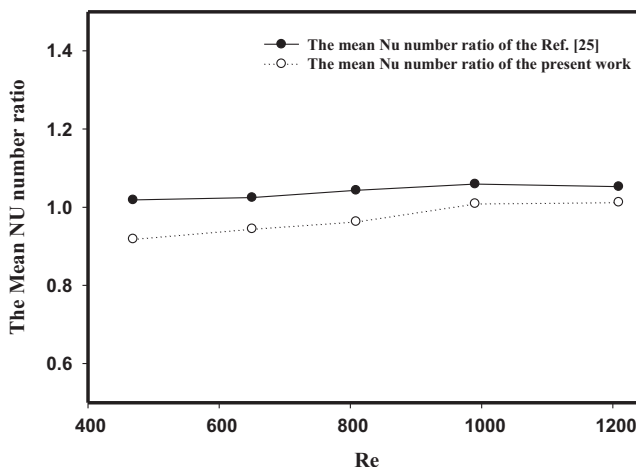


Fig. 4. The results of the comparison between the mean  $Nu$  number ratios.

water as base-fluid were used in these experiments. Also, four different Reynolds numbers and  $\phi = 0.01$  are considered. The comparison results are presented in Fig. 4 and are in good compliance. Note that the mean  $Nu$  number ratio is determined as the ratio of mean  $Nu$  number of nano-fluid to that of pure fluid.

## 5. Optimization procedure

In this section, the effects of the three effective parameters ( $Re$  number,  $\phi$  and  $dp$ ) on the convection heat transfer and nanoparticles distribution in a channel are carried out utilizing the statistical RSM model. The RSM is used to obtain the optimum status of the parameters in the computational results of the studied domain. It also contained the interaction between the mentioned parameters

[32]. The range of the model parameters variations, based on initial tests of this paper, are given as follows:

- Reynolds number ( $Re$ ):  $250 \leq Re \leq 400$ .
- The nanoparticles volume fraction ( $\phi$ ):  $0.01 \leq \phi \leq 0.05$ .
- The nanoparticles diameter ( $dp$ ):  $40 \text{ nm} \leq dp \leq 100 \text{ nm}$ .

These parameters are selected at three levels; also, based on the number of the parameters and their levels, the statistical model table (with 20 runs) is determined. The three parameters central points are achieved and the conditions of the 20 runs are defined based on the  $Re$  number,  $\phi$  and  $dp$  due to the coding; then, the tests are randomized. The values of determined test codes for the lower, equal to and higher values of the central points are assumed to be  $-1$ ,  $0$  and  $+1$ , respectively. The dependent variable in this model is considered to be the Nusselt number on the hot wall.

In RSM method, a model is defining for each dependent variable that describes the main and interaction effects of factors on each variable separately. The multivariate model is given as follows [33]:

$$Y = \beta_0 + \sum_{i=1}^3 \beta_i x_i + \sum_{i=1}^3 \beta_{ii} x_i^2 + \sum_{i=1}^3 \sum_{j=1}^3 \beta_{ij} x_i x_j \quad (25)$$

where  $\beta_0$  is the intercept,  $\beta_i$  is the linear regression coefficient of  $i$ th factor,  $\beta_{ii}$  is the quadratic regression coefficient of  $i$ th factor,  $\beta_{ij}$  is the interaction of the  $i$ th and  $j$ th factors and  $Y$  is the dependent variable.

The aim is to optimize the response of the variable  $Y$  to establish a correct relationship between independent variables and the response variable. To fit the polynomial Eq. (25), a face centered central composite design (CCF) with 20 runs, 8 cube points, 6 center points in cube and 6 axial points for 3 independent parameters, each in three levels (to estimate the percentage error of the sum of the squares) is used [34]. Parameters and their levels are summarized in Table 1. The values  $(-1)$ ,  $(0)$  and  $(+1)$  are indicated a low, middle and high level, respectively. The statistical analysis of the quadratic polynomial regression equations is carried out by using of analytical software and the related coefficients and the effects of the parameters on variables are defined. Responses and variables (as coded values) have been analyzed by design of experiment. The fitting quality of the resulted experiments has been selected or rejected applying a specific coefficient of determination and the change resources, based on the  $p$  value with 95% of certainty; finally, the answers have been analyzed utilizing analysis of variance (ANOVA).

## 6. Discussion and results

Effects of three effective parameters of the Reynolds number ( $Re$ ), volume fraction of nanoparticles ( $\phi$ ) and the nanoparticles diameter ( $dp$ ), on convective heat transfer and nanoparticles distribution, are carried out utilizing the DPM in this paper. The optimum mode is determined and the sensitivity analysis of effective parameters is performed in a channel.

### 6.1. Statistical analysis

The statistical analysis of the final 20 Runs is performed according to the determined conditions. Table 2 indicates the results of

**Table 1**  
Input variables and the levels of their values.

Variable	Symbol	-1	0	+1
Reynolds number	$Re$	250	450	650
The volume fraction of the nanoparticles	$\phi$	0.01	0.03	0.05
The nanoparticles diameter	$dp$	40 nm	60 nm	100 nm

**Table 2**

The levels of the factors values and the results of the experiments for  $Nu_{mt}$  and  $C$ .

Run order	Coded values			$Nu_{mt}$	$C$
	$Re$	$\phi$	$dp$		
1	-1	0	0	27.4002	3.0826
2	-1	1	-1	27.2166	3.3326
3	0	-1	0	39.4464	0.9405
4	-1	-1	-1	28.7112	3.2285
5	1	1	-1	85.2040	0.8005
6	-1	1	1	29.0914	3.1584
7	0	0	0	55.1418	0.9268
8	1	0	0	76.6374	0.8112
9	0	0	1	47.5438	0.9090
10	1	-1	-1	59.8882	0.8420
11	1	1	1	72.9770	0.8150
12	-1	-1	1	15.1159	3.5041
13	0	0	0	55.1218	0.9268
14	0	0	0	55.1318	0.9304
15	1	-1	1	19.1270	1.6725
16	0	0	0	55.1408	0.9269
17	0	1	0	56.8721	0.9430
18	0	0	-1	55.7045	0.9353
19	0	0	0	55.1438	0.9268
20	0	0	0	55.1428	0.9267

the mean total Nusselt number  $Nu_{mt}$  and the nanoparticles concentration ratio (the homogeneity of the nanofluid) according to the defined conditions. The nanoparticles concentration ratio ( $C$ ) is assumed to be the ratio of the nanoparticles concentration in  $Y = 0.0015$  to nanoparticles concentration at top wall.

Using the regression coefficients, the effects of the performed run conditions on dependent variables ( $Nu_{mt}$  and  $C$ ) are investigated. Tables 3 and 4 present the statistical analysis results.

According to Tables 3 and 4, the testing methods and statistical analysis of the model indicate high values of the  $R^2$  for  $Nu_{mt}$  and  $C$  (96.67% and 99.24%, respectively) which shows that this model is appropriate for calculating the values of the Nusselt number and nanoparticles concentration ratio. However, the amounts of the  $R^2 - adj$  for  $Nu_{mt}$  and  $C$  (94.72% and 98.80% respectively) are less than  $R^2$ , but the model fits the experimental data satisfactorily [35]. The Meaningfulness of the model for Nusselt number and nanoparticles concentration ratio is expressed by  $F$ , which is equal to 49.70 and 224.97, respectively; since, the  $F$ -value is not caused by noise.

### 6.2. Analysis of variance and model estimation

The estimated regression and statistical analysis of experimental models are carried out in this section due to the simulation studies which are considered under different experimental compounds. Figs. 5 and 6 show the obtained residual plots due to entering the data into analytical software and analyzing of variance (ANOVA).

By considering of Figs. 5 and 6, normal probability plots of residuals are in good conditions [35]. In addition, Residual Histograms have skewed distribution in these two figures, and are not similar to a symmetrical distribution. Comparing the residual diagrams and fitted values shows a good correlation between observed and fitted values. The highest residuals among all responses are observed to be in the proximity of 7.00 and 0.15 for  $Nu_{mt}$  and  $C$ , respectively.

The general form of the relationship between the effective test parameters and the variations of the mean total Nusselt number and the nanoparticles concentration ratio is available in Eq. (26) which is obtained as uncoded units by applying the response surface methodology (RSM) as follows:

$$Nu_{mt} \text{ and } C = A + B^* Re + C^* \phi + D^* dp + E^* Re^* Re + F^* \phi^* \phi + G^* dp^* dp + H^* Re^* \phi + I^* Re^* dp + J^* \phi^* \phi \quad (26)$$

**Table 3**

The analysis results of the variance for the  $Nu_{mt}$ .

Source	DOF	Adj. sum of squares (SS)	Adj. mean squares (MS)	F-value	P-value	
Model	7	6747.75	963.96	49.70	<0.000	Significant
Linear	3	5191.38	1730.46	89.22	<0.000	
Square	1	545.59	545.59	28.13	<0.000	
2-way Interaction	3	1010.78	336.93	17.37	<0.000	
Error	12	232.74	19.40	–	–	
Lack-of-fit	7	232.74	33.25	442928.45	<0.000	Significant
Pure error	5	0.00	0.00	–	–	
Total	19	6980.49	–	–	–	

$R^2 = 96.67\%$ ,  $R^2 - adj = 94.72\%$ .

**Table 4**

The analysis results of the variance for C.

Source	DOF	Adj. sum of squares (SS)	Adj. mean squares (MS)	F-value	P-value	
Model	7	20.6010	2.9430	224.97	<0.000	Significant
Linear	3	13.1311	4.3770	334.59	<0.000	
Square	1	7.1465	7.1465	546.30	<0.000	
2-way Interaction	3	0.3234	0.1078	8.24	<0.003	
Error	12	0.1570	0.0131	–	–	
Lack-of-fit	7	0.1570	0.0224	10375.02	<0.000	Significant
Pure error	5	0.0000	0.0000	–	–	
Total	19	20.7580	–	–	–	

$R^2 = 99.24\%$ ,  $R^2 - adj = 98.80\%$ .

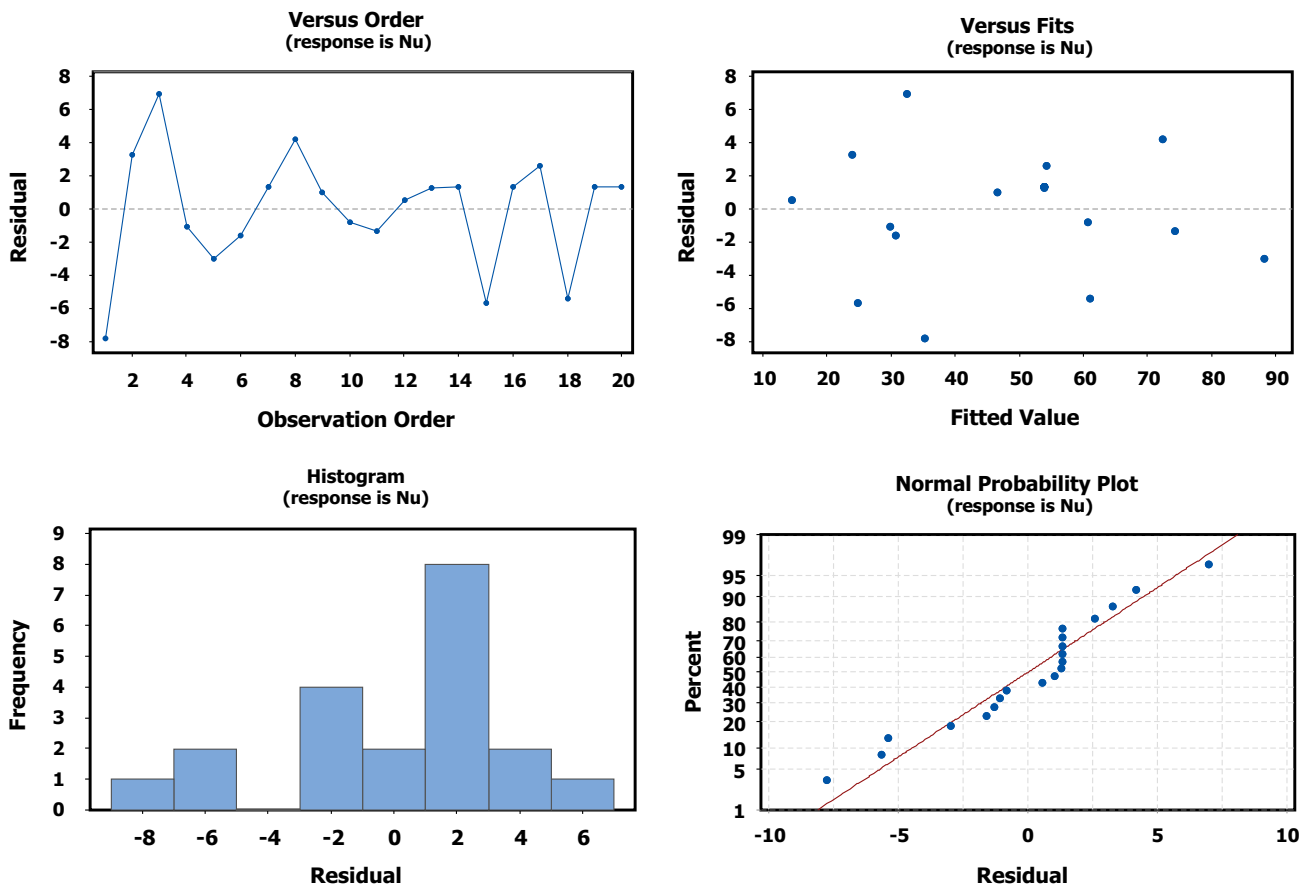


Fig. 5. Residual plots of  $Nu_{mt}$ .

Table 5 presents the coefficients in Eq. (26) for the mean total Nusselt number and nanoparticles concentration ratio after removing insignificant amounts according to the  $P$ -value [36,37].

Eqs. (27) and (28) indicate the relationship between the variations of the mean total Nusselt number and the nanoparticles

concentration ratio, and the effective test parameters as coded units. Only meaningful coefficients are considered in these equations.

$$Nu_{mt} = 53.81 + 18.63Re + 10.91\Phi - 7.29dp - 10.45\Phi * \Phi + 8.34Re * \Phi - 5.16Re * dp + 5.50\Phi * dp \quad (27)$$

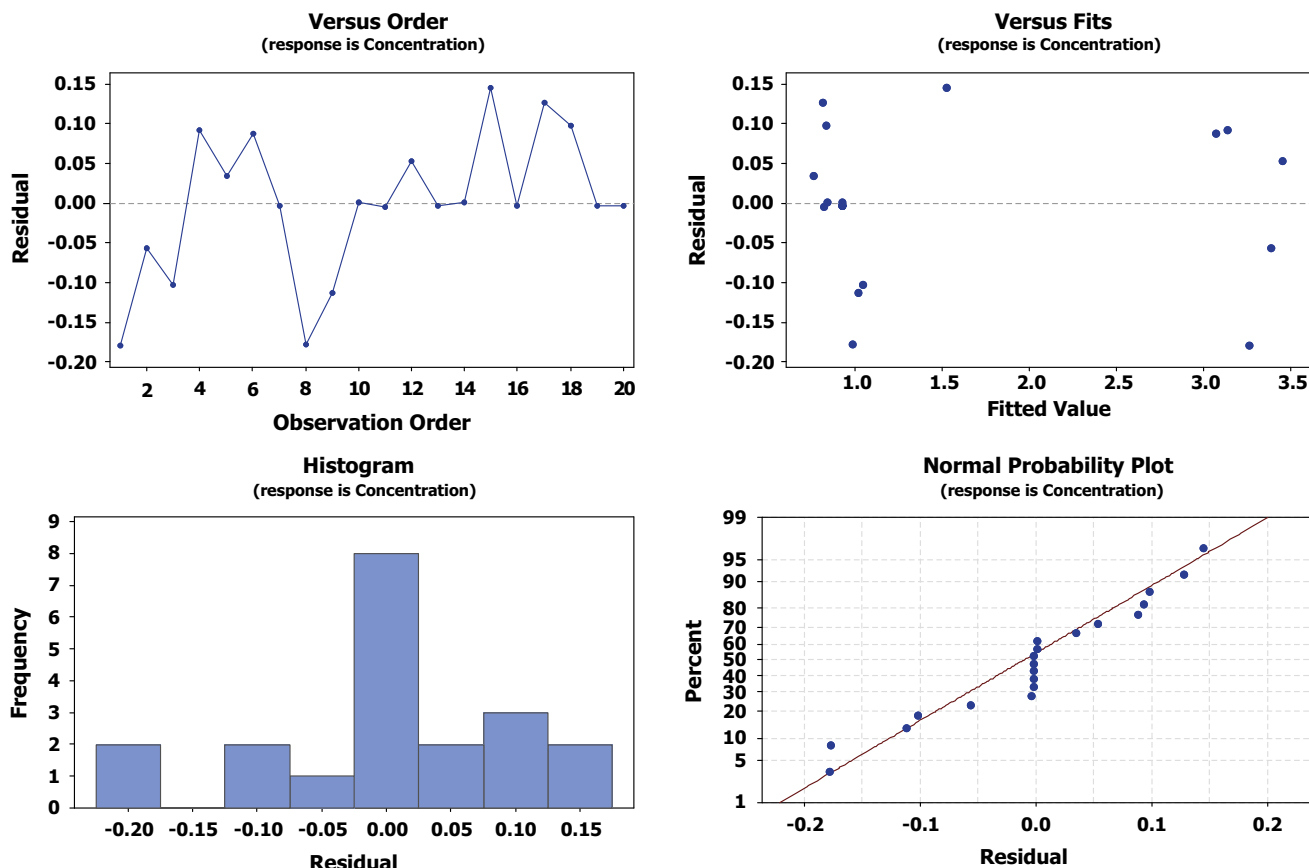


Fig. 6. Residual plots of C.

**Table 5**  
Estimated regression coefficients.

Term	Coefficient of $Nu_{mt}$	Coefficient of C
A	53.81	0.9292
B	18.63	-1.1365
C	10.91	-0.1138
D	-7.29	0.0920
E	0.000	1.1955
F	-10.45	0.0000
G	0.00	0.0000
H	8.34	-0.0822
I	-5.16	0.0930
J	5.50	-0.1582

$$C = 0.9292 - 1.1365Re - 0.1138\phi + 0.0920dp + 1.1955Re * Re - 0.0822Re * \phi + 0.0930Re * dp - 0.1582\phi * dp \quad (28)$$

The variations of the mean total Nusselt number and the nanoparticles concentration ratio, as effective parameters functions are shown in Figs. 7 and 8, respectively, as follows:

Figs. 7 and 8 indicate the variations of the mean total Nusselt number and the nano-particles concentration in terms of the  $Re$  number and  $\phi$  (a),  $Re$  number and  $dp$  (b) and  $\phi$  and  $dp$  (c), respectively.

According to Fig. 7, it can be concluded that:

- (a) Increasing the  $Re$  number and  $\phi$  enhances the mean total Nusselt number and its highest values are observed in levels of (+1) and (0) and its lowest in level of (-1) for the  $Re$  number and  $\phi$ , respectively.

- (b) An enhancement in the  $Re$  number and reducing of  $dp$  increase the mean total Nusselt number and its highest values are observed in levels of (+1) and (-1) and its lowest in (-1) and (+1) for the  $Re$  number and  $dp$ , respectively.
- (c) By increasing the  $\phi$  and reduction of  $dp$  the mean total Nusselt number increases, and its highest values are observed in levels of (0) and (-1) and its lowest in (-1) and (+1) for the  $\phi$  and  $dp$ , respectively.
- (d) As mentioned in introduction section, the thermal conductivity increases with increasing of volume fraction of nanoparticles, thus the heat transfer rate increases. Therefore, by increasing of the Reynolds number, the mean Nusselt number increases with  $\phi$ . On the other hand, the effects of the Reynolds number, nanoparticle volume fraction and nanoparticles diameter on Nusselt number are available in Fig. 7. Enhancement of the energy transport in the fluid with the volume fraction increases the velocity components of nanofluid. In addition, the sensitivity of the thermal boundary layer thickness to nanoparticles volume fraction is related to the increased thermal conductivity of the nanofluid. In fact, higher values of thermal conductivity occur with higher values of thermal diffusivity, which reduces the temperature gradients and thus enhances the boundary layer thickness. The Nusselt number increases due to this enhancement in thermal boundary layer thickness. Because as mentioned above, increasing in volume fraction decreases the temperature gradients and according to Eq. (18) enhances the mean  $Nu$  number. Increasing of the mean  $Nu$  number with the Reynolds number and nanoparticles volume fraction is also observed in Ref. [19].



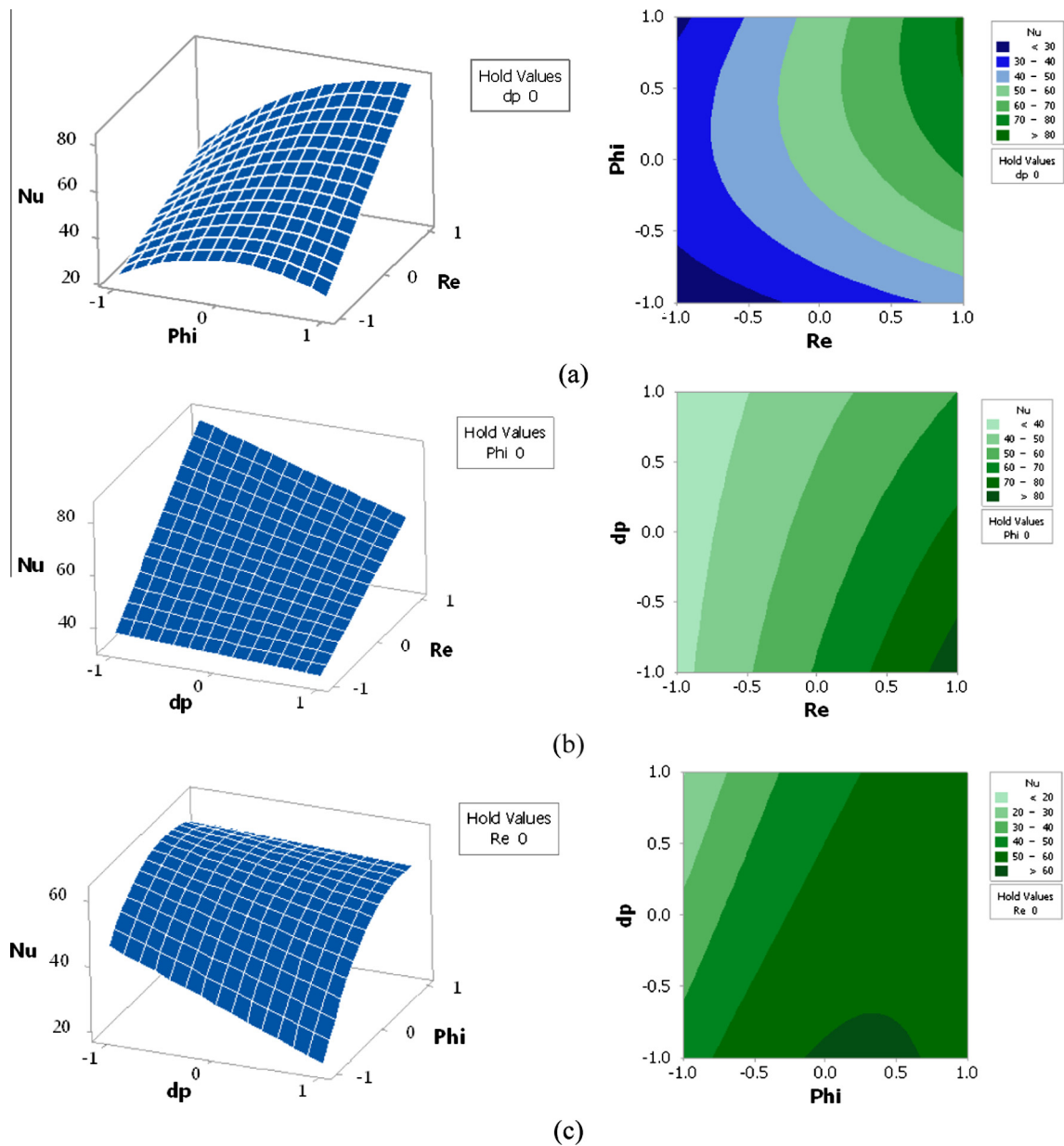


Fig. 7. The variations of the  $Nu_{m}$  as a function of effective parameters (a)  $Re$ - $\Phi$ , (b)  $Re$ - $dp$  and (c)  $\Phi$ - $dp$ .

(e) By enhancement in particle size, lower heat transfer increases are observed, which is due to the attenuation in the nanoparticles Brownian motion. In addition, for particles with small diameter, Particle diameter has a considerable effect on heat transfer enhancement [38]. A more in-depth discussion about the effects of  $d_p$  on heat transfer is available in the recently published paper [10].

In addition, following results can be obtained from Fig. 8:

- (a) Reduction of the  $Re$  number and increasing in  $\Phi$ , enhances the nanoparticles concentration ratio and its highest values are observed in levels of  $(-1)$  and  $(+1)$  and its lowest in  $(0)$  and  $(-1)$  for the  $Re$  number and  $\Phi$ , respectively.
- (b) By decreasing of the  $Re$  number and increasing of  $dp$  the nanoparticles concentration ratio enhances and its highest values are observed in levels of  $(-1)$  and  $(+1)$  and its lowest in  $(+1)$  and  $(-1)$  for the  $Re$  number and  $dp$ , respectively.

(c) An Increase in  $dp$  and  $\Phi$  enhances the nanoparticles concentration ratio and its highest value is observed in level of  $(+1)$  and its lowest in  $(-1)$  for the  $dp$  and  $\Phi$ .

(d) Increasing of the nanoparticles diameter reduces the Brownian motion effect, and as a result, decreases the distribution of the nanoparticles in the channel; also, the nanoparticles concentration in  $Y = 0.0015$  increases more than that of the case with smaller nanoparticles diameter and thus smaller Brownian motion effect. This is because of the reduction in nanoparticles movement, and the higher concentration of nanoparticles in bottom part of the channel compared to its upper part due to the gravity force. Thus, according to the description of the homogeneity which have mentioned above, the ratio of the nanoparticles concentration in  $Y = 0.0015$  to nanoparticles concentration at top wall, increases; and as a result the nanoparticles with higher diameters, will have more homogeneity. A more in-depth discussion about the effects of  $d_p$  on heat transfer is available in the recently published paper [38].

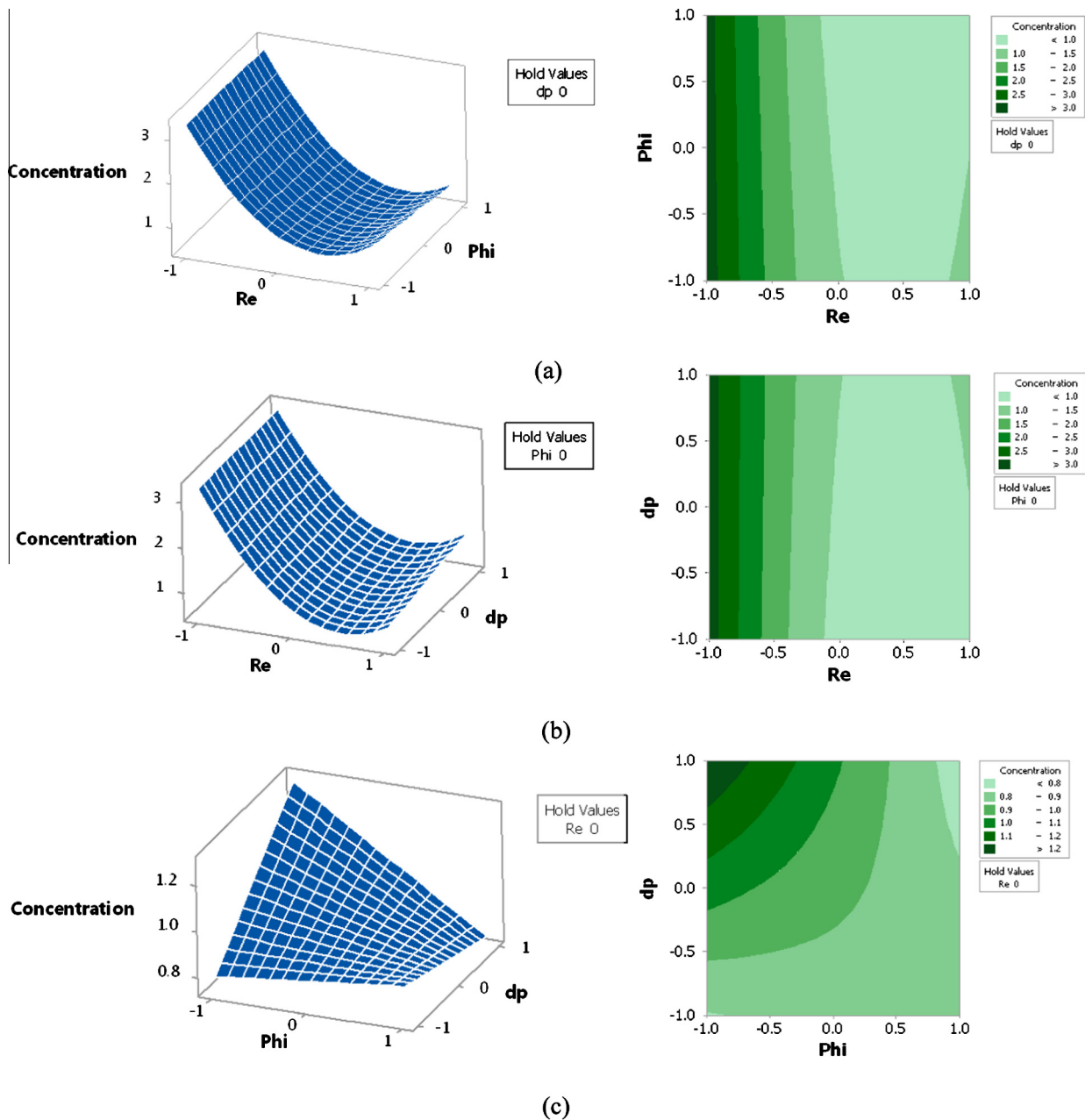


Fig. 8. The variations of the  $C$  as a function of effective parameters (a)  $Re-\Phi$ , (b)  $Re-dp$  and (c)  $\Phi-dp$ .

(e) With increasing of the nanoparticles volume fraction, the mentioned ratio (nanoparticles concentration ratio) increases and as a result the homogeneity enhances.

## 7. Sensitivity analysis

The sensitivity analysis plays a significant role in computational and simulation models. Understanding of the model outputs sensitivity to the disturbances in the model inputs is absolutely necessary [39] while the model parameters, input variables and the values of the calculations are inclined to different uncertainty sources. Therefore, developing numerical simulation method may be carried out to study models [40] by the means of the sensitivity analysis mathematical and computational concepts. To obtain the sensitivity of the model outputs to the uncertainty of the parameter values, input variables and the calculations, the sensitivity analysis tests on mathematical and computational models is performed

[39]. By using of the results of these tests, the most effective parameters or input values on the model outputs are specified. The derivative of the output variables to input parameters are calculated to define the sensitivity of the mean total Nusselt number and the nanoparticles concentration ratio as output variables to effective input parameters of the  $Re$  number,  $\Phi$  and  $dp$ . Thus, the derivative of Eqs. (27) and (28) to input variables are computed, which are the mean total Nusselt number and the nanoparticles concentration ratio, respectively, and can be given as follows:

$$\frac{\partial Nu_{mt}}{\partial Re} = 18.63 + 8.34 * \Phi - 5.16 * dp \quad (29)$$

$$\frac{\partial Nu_{mt}}{\partial \Phi} = 10.91 - 20.90 * \Phi + 8.34 * Re + 5.50 * dp \quad (30)$$

$$\frac{\partial Nu_{mt}}{\partial dp} = -7.29 - 5.16 * Re + 5.50 * \Phi \quad (31)$$

$$\frac{\partial C}{\partial Re} = -1.1365 + 2.391 * Re - 0.0822 * \Phi + 0.0930 * dp \quad (32)$$

$$\frac{\partial C}{\partial \phi} = -0.1138 - 0.0822 * Re - 0.1582 * dp \quad (33)$$

$$\frac{\partial C}{\partial dp} = 0.0920 + 0.0930 * Re - 0.1582 * \Phi \quad (34)$$

Eqs. (29)–(31) and (32)–(34) are related to the mean total Nusselt number and the nanoparticles concentration ratio, respectively.

The positive value of the sensitivity means an increase in the objective function due to increasing of input parameters. Also the negative value of the sensitivity represents a decrease in the objective function caused by increasing of the input parameters. Tables 6 and 7 indicate the results of the sensitivity analysis. Note that the values in the tables are obtained for a channel with the *Re* number at levels -1, 0 and +1 (250, 450 and 650), the volume fraction of nanoparticles  $\phi$  with levels 0 and +1 (0.03 and 0.05) and *dp* at level +1 (100 nm).

Figs. 9 and 10 present the sensitivity of the mean total Nusselt number and nanoparticles concentration ratio to the effective input parameters, respectively, as follows:

By considering of Fig. 9 and Table 6, the sensitivity of the mean total Nusselt number to the *Re* number and  $\phi$  is positive but to *dp* is negative. In addition, by increasing of the *Re* number levels, the sensitivity of the mean *Nu* number to  $\phi$  increases and its sensitivity

**Table 6**  
The sensitivity analysis for  $Nu_{mt}$ .

<i>Re</i>	$\phi$	<i>d</i>	Sensitivity		
			$\frac{\partial Nu_{mt}}{\partial Re}$	$\frac{\partial Nu_{mt}}{\partial \phi}$	$\frac{\partial Nu_{mt}}{\partial dp}$
-1	-1	-1	15.45	17.97	-7.63
0	-1	-1	15.45	26.31	-12.79
+1	-1	-1	15.45	36.65	-17.95

**Table 7**  
The sensitivity analysis for *C*.

<i>Re</i>	$\phi$	<i>d</i>	Sensitivity		
			$\frac{\partial C}{\partial Re}$	$\frac{\partial C}{\partial \phi}$	$\frac{\partial C}{\partial dp}$
-1	-1	-1	-3.5383	0.1266	0.1572
0	-1	-1	-1.1473	0.0444	0.2502
+1	-1	-1	1.2437	-0.0387	0.3432

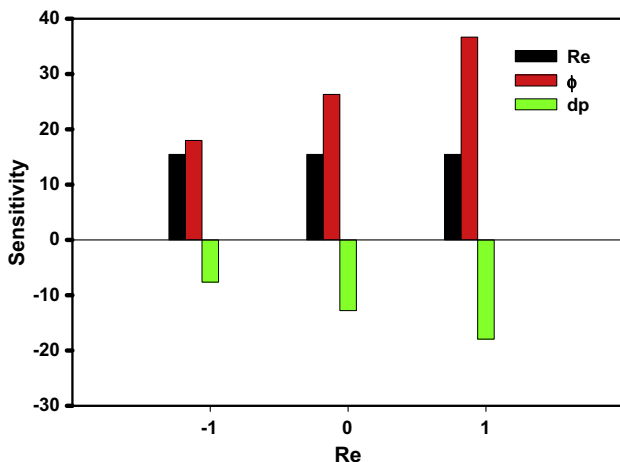


Fig. 9. The sensitivity analysis results of the  $Nu_{mt}$  ( $\phi$  and *dp* in level -1).

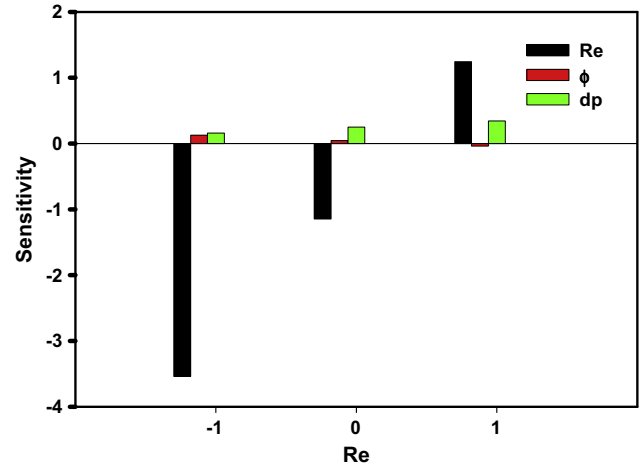


Fig. 10. The sensitivity analysis results of the *C* ( $\phi$  and *dp* in level -1).

to *dp* decreases. Since, increasing in the *Re* number and  $\phi$  and reduction of *dp*, enhances the mean total Nusselt number (It is consistent with Fig. 7).

However, according to Fig. 10 and Table 7, the sensitivity of the nanoparticles concentration ratio *C* (the nano-fluid homogeneity) to the *Re* number is negative but to  $\phi$  and *dp* is positive, which means that increasing the *Re* number decreases the homogeneity of nano-fluid but an enhancement in  $\phi$  and *dp* makes the mixture more homogeneous (It is consistent with Fig. 8).

In addition, the sensitivity of the mean Nusselt number to the *Re* number,  $\phi$  and *dp* parameters is more than the sensitivity of the nanoparticles concentration ratio to these parameters.

### 8. Conclusions

The convection heat transfer and the nanoparticles concentration distribution (homogeneity) in a channel have been investigated numerically using the Discrete Phase Model. The top and bottom walls of the channel are assumed to be adiabatic except for a part of the bottom wall which is under a uniform heat flux  $q''$ . Numerical simulations have been carried out to study the effects of the three parameters, the Reynolds number ( $50 \leq Re \leq 250$ ), nanoparticles volume fraction ( $0.01 \leq \phi \leq 0.05$ ) and the nanoparticles diameter ( $40 \text{ nm} \leq d \leq 100 \text{ nm}$ ), on the heat transfer performance and nanoparticles distribution inside the channel. The mean total Nusselt number and the nanofluid homogeneity have been calculated and the residual diagrams have been obtained in order to define the optimum conditions for a better heat transfer and nanofluid homogeneity. Finally, using the sensitivity analysis, the effects of the above mentioned effective parameters on the mentioned functions have been studied. The obtained results of the numerical study have been summarized as the following:

- Increasing the *Re* number and  $\phi$  enhances the mean total Nusselt number and its highest values are observed in levels of (+1) and (0) and its lowest in level of (-1) for the *Re* number and  $\phi$ , respectively.
- Reduction of *dp* increase in the mean total Nusselt number and its highest value is observed in level of (-1) and its lowest in (+1) for *dp*.
- By Decreasing of the *Re* number and increasing of  $\phi$  the nanoparticles concentration ratio enhances and its highest values are observed in levels of (-1) and (+1) and its lowest in (0) and (-1) for the *Re* number and  $\phi$ , respectively.

- An enhancement in  $dp$  increases the nanoparticles concentration ratio and its highest value is observed in level of (+1) and its lowest in (−1) for  $dp$ .
- The sensitivity of the mean total Nusselt number to the  $Re$  number and  $\phi$  is positive but to  $dp$  is negative. Since, increasing in the  $Re$  number and  $\phi$  and reduction of  $dp$ , enhances the mean total Nusselt number
- By increasing of the  $Re$  number levels, the sensitivity of the mean  $Nu$  number to  $\phi$  increases and its sensitivity to  $dp$  decreases.
- the sensitivity of the nanoparticles concentration ratio to the  $Re$  number is negative but to  $\phi$  and  $dp$  is positive, which means that increasing the  $Re$  number decreases the homogeneity of nano-fluid but an enhancement in  $\phi$  and  $dp$  makes the mixture more homogeneous.
- The sensitivity of the mean total Nusselt number to  $Re$  number,  $\phi$  and the  $dp$  parameters is more than the sensitivity of the nanoparticles concentration ratio to these parameters.

## References

- [1] M. Mamourian, K. Milani Shirvan, R. Ellahi, A.B. Rahimi, Optimization of mixed convection heat transfer with entropy generation in a wavy surface square lid-driven cavity by means of Taguchi approach, *Int. J. Heat Mass Transfer* 102 (2016) 544–554.
- [2] V. Bianco, O. Manca, S. Nardini, Performance analysis of turbulent convection heat transfer of  $Al_2O_3$  water-nanofluid in circular tubes at constant wall temperature, *Energy* 77 (2014) 403–413.
- [3] M. Siavashi, H.R. TaleshBahrami, H. Saffari, Numerical investigation of flow characteristics, heat transfer and entropy generation of nano-fluid flow inside an annular pipe partially or completely filled with porous media using two-phase mixture model, *Energy* 93 (2015) 2451–2466.
- [4] V. Bianco, O. Manca, S. Nardini, Entropy generation analysis of turbulent convection flow of  $Al_2O_3$ -water nanofluid in a circular tube subjected to constant wall heat flux, *Energy Convers. Manage.* 77 (2014) 306–314.
- [5] D. Huang, Z. Wu, B. Sunden, Pressure drop and convective heat transfer of  $Al_2O_3$ /water and MWCNT/water nano-fluids in a chevron plate heat exchanger, *Int. J. Heat Mass Transfer* 89 (2015) 620–626.
- [6] D. Haridas, N.S. Rajput, A. Srivastava, Interferometric study of heat transfer characteristics of  $Al_2O_3$  and  $SiO_2$ -based dilute nanofluids under simultaneously developing flow regime in compact channels, *Int. J. Heat Mass Transfer* 88 (2015) 713–727.
- [7] M. Rahimi-Gorji, O. Pourmehran, M. Hatami, D.D. Ganji, Statistical optimization of micro-channel heat sink (MCHS) geometry cooled by different nanofluids using RSM analysis, *Eur. Phys. J. Plus* 130 (2) (2015) 1–21.
- [8] Y.L. Zhai, G.D. Xia, X.F. Liu, Y.F. Li, Heat transfer enhancement of  $Al_2O_3$ - $H_2O$  nanofluids flowing through a micro heat sink with complex structure, *Int. Commun. Heat Mass Transfer* 66 (2015) 158–166.
- [9] E. Ebrahimi-Bajestan, M. CharjouiMoghadam, H. Niazmand, W. Daungthongsuk, S. Wongwises, Experimental and numerical investigation of nano-fluids heat transfer characteristics for application in solar heat exchangers, *Int. J. Heat Mass Transfer* 92 (2016) 1041–1052.
- [10] C. Qi, L. Liang, Zh. Rao, Study on the flow and heat transfer of liquid metal based nano-fluid with different nanoparticle radiuses using two-phase lattice Boltzmann method, *Int. J. Heat Mass Transfer* 94 (2016) 316–326.
- [11] A. Malvandi, S.A. Moshizi, D.D. Ganji, Two-component heterogeneous mixed convection of alumina/water nanofluid in microchannels with heat source/sink, *Adv. Powder Technol.* 27 (1) (2016) 245–254.
- [12] S. Mirfendereski, A. Abbassi, M. Saffar-avval, Experimental and numerical investigation of nanofluid heat transfer in helically coiled tubes at constant wall heat flux, *Adv. Powder Technol.* 26 (5) (2015) 1483–1494.
- [13] Ch. Abdellahoum, A. Mataoui, H.F. Oztop, Comparison of viscosity variation formulations for turbulent flow of  $Al_2O_3$ -water nanofluid over a heated cavity in a duct, *Adv. Powder Technol.* 26 (4) (2015) 1210–1218.
- [14] A. Malvandi, D.D. Ganji, Effects of nanoparticle migration on forced convection of alumina/water nanofluid in a cooled parallel-plate channel, *Adv. Powder Technol.* 25 (4) (2014) 1369–1375.
- [15] F. Selimefendigil, H.F. Oztop, N. Abu-Hamdeh, Mixed convection due to rotating cylinder in an internally heated and flexible walled cavity filled with  $SiO_2$ -water nanofluids: effect of nanoparticle shape, *Int. Commun. Heat Mass Transfer* 71 (2016) 9–19.
- [16] K. Jin, Modeling nanoparticle migration in pipe flow through Eulerian-Lagrangian approach, a thesis presented to the graduate and research committee of Lehigh University for the degree of Master of Science, 2011.
- [17] H. Afshar, M. Shams, S.M.M. Nainian, G. Ahmadi, Micro-channel heat transfer and dispersion of nanoparticles in slip flow regime with constant heat flux, *Int. Commun. Heat Mass Transfer* 36 (2009) 1060–1066.
- [18] H. Aminfar, R. Motallebzadeh, Investigation of the velocity field and nanoparticle concentration distribution of nano-fluid using Lagrangian-Eulerian approach, *J. Dispersion Sci. Technol.* 33 (2012) 155–163.
- [19] V. Bianco, F. Chiacchio, O. Manca, S. Nardini, Numerical investigation of nano-fluids forced convection in circular tubes, *Appl. Therm. Eng.* 29 (2009) 3632–3642.
- [20] Y.J. Chen, Y.Y. Li, Zh.H. Liu, Numerical simulations of forced convection heat transfer and flow characteristics of nano-fluids in small tubes using two-phase models, *Int. J. Heat Mass Transfer* 78 (2014) 993–1003.
- [21] D. Li, K. Luo, J. Dang, A moving boundary model for two-phase flow heat exchanger incorporated with relative velocities between boundaries and fluid, *Int. J. Heat Mass Transfer* 95 (2016) 35–44.
- [22] M. Rahimi-Gorji, O. Pourmehran, M. Gorji-Bandpy, T.B. Gorji, CFD simulation of airflow behavior and particle transport and deposition in different breathing conditions through the realistic model of human airways, *J. Mol. Liq.* 209 (2015) 121–133.
- [23] M. Mamourian, K. Milani Shirvan, S. Mirzakhani, A.B. Rahimi, Vortex generators position effect on heat transfer and nanofluid homogeneity: a numerical investigation and sensitivity analysis, *Appl. Thermal Eng.*, <http://dx.doi.org/10.1016/j.applthermaleng.2016.07.068>.
- [24] A. abdollahi, M. Shams, Optimization of heat transfer enhancement of nanofluid in a channel with winglet vortex generator, *Applied Thermal Engineering*; 10.1016/j.applthermaleng.2015.08.066.
- [25] W.J. Minkowycz, E.M. Sparrow, J.Y. Murthy, *Handbook of Numerical Heat Transfer*, John Wiley & Sons, Hoboken, NJ, 2006.
- [26] W.E. Ranz, W.R. Marshall, Evaporation from drops, part I, *Chem. Eng. Prog.* 48 (3) (1952) 141–146.
- [27] H. Ounis, G. Ahmadi, J.B. McLaughlin, Brownian diffusion of sub-micrometer particles in the viscous sublayer, *J. Colloid Interface Sci.* 143 (1) (1991) 266–277.
- [28] P.G. Saffman, The lift on a small sphere in a slow shear flow, *J. Fluid Mech.* 22 (1965) 385–400.
- [29] L. Talbot, R.K. Cheng, R.W. Schefer, D.R. Willis, Thermophoresis of particles in a heated in heated boundary layer, *J. Fluid Mech.* 101 (pt 4) (1980) 737–758.
- [30] A. Li, G. Ahmadi, Dispersion and deposition of spherical particles from point sources in a turbulent channel flow, *Aerosol Sci. Technol.* 16 (1992) 209–226.
- [31] M.M. Heyhat, F. Kowsary, A.M. Rashidi, M.H. Momenpour, A. Amrollahi, Experimental investigation of laminar convective heat transfer and pressure drop of water- based  $Al_2O_3$  nano-fluids in fully developed flow regime, *Exp. Thermal Fluid Sci.* 44 (2013) 483–489.
- [32] R.H. Myers, A.L. Khuri, G. Vining, Response surface alternatives to the Taguchi robust parameter design approach, *Am. Stat.* 46 (1992) 131–136.
- [33] W.P. Gardiner, G. Gettinby, *Experimental Design Techniques in Statistical Practice: A Practical Software-Based Approach*, Harwood, England, 1998.
- [34] G.E.P. Box, J.S. Hunter, Multi-factor experimental designs for exploring response surfaces, *Ann. Math. Stat.* 28 (1975) 195–241.
- [35] H. Joardar, N.S. Das, G. Sutradhar, An experimental study of effect of process parameters in turning of LM6/ $SiC_p$  metal matrix composite and its prediction using response surface methodology, *Int. J. Eng. Sci. Technol.* 3 (8) (2011) 132–141.
- [36] M. Mamourian, K. Milani-Shirvan, S. Mirzakhani, Two phase simulation and sensitivity analysis of effective parameters on turbulent combined heat transfer and pressure drop in a solar heat exchanger filled with nanofluid by Response Surface Methodology, *Energy* 109 (2016) 49–61.
- [37] K. Milani Shirvan, M. Mamourian, S. Mirzakhani, R. Ellahi, Two phase simulation and sensitivity analysis of effective parameters on combined heat transfer and pressure drop in a solar heat exchanger filled with nanofluid by RSM, *J. Mol. Liq.* 220 (2016) 888–901.
- [38] J. Koo, K. Kleinstreuer, A new thermal conductivity model for nanofluids, *J. Nanopart. Res.* 6 (6) (2004) 577–588.
- [39] F. Campolongo, R. Braddock, The use of graph theory in sensitivity analysis of model output: a second order screening method, *Reliab. Eng. Syst. Quantitative, model independent method for global sensitivity analysis of model output* *Technometrics* 411999 39–56.